

Evaluation of Assumptions Made by Hygroscopic Tandem Differential Mobility Analyzer Inversion Routines

In preparation for submission to
Journal of Aerosol Science

Christopher R. Oxford^{1,2,}, Rajan K. Chakrabarty^{1,2}, and Brent J. Williams^{1,2}*

¹ *Department of Energy, Environmental, and Chemical Engineering, Washington University in St. Louis, St. Louis, Missouri 63130*

² *Center for Aerosol Science & Engineering (CASE), Washington University in St. Louis, St. Louis, Missouri 63130*

* Corresponding Author.

E-mail address: coxford@wustl.edu; Postal address: 1 Brookings Drive, Campus Box 1180, Saint Louis, MO 63130 United States of America

Highlights

- Traditional inversion routines used for Hygroscopic Tandem Differential Mobility Analyzer (H-TDMA) experiments can create spurious trends as a function of diameter or experimental time.
- Multiply-charged particles grow less than singly-charged particles with the same growth factor.
- A single growth factor distribution describes grass burning aerosol from 120 nm to 241 nm.
- Multicharged inversion, correcting for Slope and Multicharged Dispersion biases, generates higher hygroscopicities than traditional inversion routines.

Graphical Abstract

Keywords

Hygroscopicity; Inversion; Multicharging; Hygroscopic Tandem Differential Mobility Analyzer; HTDMA bias

Abstract

The Hygroscopic Tandem Differential Mobility Analyzer (H-TDMA) measures the hygroscopicity of atmospheric particles, and many atmospheric processes that change this hygroscopicity also change the atmospheric size distribution. Two assumptions made during H-TDMA inversion create spurious hygroscopic trends as a function of the changing inlet size distribution. These two assumptions—that the particles exiting the first Differential Mobility Analyzer (DMA1) are singly charged and that the inlet size distribution has a slope of zero (flat)—generate Multi-Charge Dispersion (MCD) bias and Slope bias, respectively. First, we use a model, named TAO, to show that the inlet size distribution could theoretically change the measured ammonium sulfate hygroscopicity by 10% to 20% as a function of diameter or experimental time with no change in relative humidity. Secondly, we show experimentally that aerosol emitted from the flaming combustion of grass creates MCD bias. In this experiment, we measure the CPC response of the first three charges and invert these responses using a new routine named Junior. Junior's inversion of each charge shows that one growth factor distribution describes all measured diameters (no growth dependence on diameter). As in the modeling study above, previous publications of this aerosol system, using traditional inversion assumptions, report a decrease in hygroscopicity as DMA1 diameter increases. Unlike traditional inversions, Junior's inversion does not assume the particles are singly charged nor does it make the flat inlet size distribution assumption. Instead, both the inlet size distribution and each charge's CPC response are measured quantities. Thus, the discrepancy between our inversion results and previous publications is likely due to the traditional inversion routine assumptions. This underscores the importance for accounting for Slope and MCD bias during inversions. Experimental results should be carefully analyzed when reporting hygroscopic trends with respect to diameter or experimental time when using the traditional inversion assumptions.

1. Introduction

Atmospheric particles play a major role in the Earth's climate system through both direct interactions with solar radiation and indirect interactions through cloud activation (Schwartz, 2018; Schwartz, Charlson, Kahn, Ogren, & Rodhe, 2010). The indirect interaction is the greater of the two effects (Regayre et al., 2014; Stocker et al., 2014) and is influenced by the activation of aerosols into cloud droplets (Köhler, 1936). This cloud droplet activation has both a size and a composition dependence (Farmer, Cappa, & Kreidenweis, 2015). For size, the dry particle and the water droplet are assumed to be spherical, and diameter specifies the size. For composition, the droplet solution is assumed ideal, and dry particle diameter, droplet diameter, and hygroscopicity (Markus D. Petters & Kreidenweis, 2007) specifies the activity of water. Assuming a spherical particle and an ideal solution enables diameter-based instruments to contribute to the study of cloud droplet activation (Chuang, Nenes, Smith, Flagan, & Seinfeld, 2000; Roberts & Nenes, 2005; Snider, Petters, Wechsler, & Liu, 2006).

The Hygroscopic Tandem Differential Mobility Analyzer (H-TDMA) is a diameter-based instrument that measures the change in diameter due to an increase in relative humidity (Johnson, Fletcher, Meyer, Modini, & Ristovski, 2008; Lopez-Yglesias, Yeung, Dey, Brechtel, & Chan, 2014; Villani, Picard, Michaud, Laj, & Wiedensohler, 2008). The H-TDMA first selects an aerosol from an inlet size distribution using the first of two Differential Mobility Analyzers (DMA1), which selects particle sizes based on electrical mobility. The selected aerosol flows through a humidifier, and the aerosol grows to a larger size due to the absorbance of water. The second Differential Mobility Analyzer (DMA2), in combination with a Condensation Particle Counter (DMA2 CPC), measures the final size of the aerosol particles (Liu et al., 1978; McMurry & Stolzenburg, 1989). The measured DMA2 CPC response is the convolution of the selected size distributions exiting DMA1 with both the hygroscopic growth of the particles and the integrated response from the DMA2 CPC.

The measured data must be inverted to determine the desired particle growth factor distribution (Gysel, McFiggans, & Coe, 2009). This inversion process deconvolves the DMA2 CPC response using the DMA1 and DMA2 transfer functions and assumptions about the inlet size distribution (Stolzenburg, 2018). A number of H-TDMA data inversion routines exist to date (Cubison, Coe, & Gysel, 2005; Gysel et al., 2009; Markus D Petters, 2018; Stolzenburg, 2018; Stratmann, Orsini, & Kauffeldt, 1997; Voutilainen, Stratmann, & Kaipio, 2000), and it is of interest to determine if assumptions applied in traditional routines are susceptible to biases or errors in their determination of growth properties of humidified particle distributions.

Traditional inversion routines make two assumptions about the inlet size distribution, which allow the inlet size distribution to be neglected, simplifying inversion. First, the inlet size distribution is assumed flat over the narrow width of the DMA1 transfer function, and the selected size distributions exiting DMA1 have the shape of the DMA1 transfer function. The second assumption is that the selected size distribution can be assumed singly charged, and the multiple selected size distributions (each corresponding with a charge) are reduced to only the singly-charged selected size distribution. The first inversion routines (Stolzenburg, 2018) allowed input of the total number of particles exiting DMA1, measured by a CPC between DMA1 and DMA2 (Hennig, Massling, Brechtel, & Wiedensohler, 2005), known further as the DMA1 CPC. With the total number of particles and the shape of the selected size distribution known, the singly-charged selected size distribution becomes fully defined without knowledge of the inlet size distribution. Then the inversion process, employing the DMA transfer functions and the DMA2 CPC response, returns the growth factor distribution (Stolzenburg & McMurry,

2008). The new inversion routine by Markus D Petters (2018) does consider the inlet size distribution and has a distinct influence on this study as included below.

Many H-TDMAs omit the DMA1 CPC and focus on the growth of the aerosol (Hakala, Mikkilä, Hong, Ehn, & Petäjä, 2017; Hennig et al., 2005; Oxford et al., 2019). When the growth factor distribution is integrated, the penetration fraction is calculated, and this penetration fraction appears to be the primary benefit of the DMA1 CPC. This penetration fraction represents the ratio of the actual transmitted particles to the selected total population. Hygroscopic relationships use the growth factor (not penetration) to establish hygroscopicity (Markus D. Petters & Kreidenweis, 2007). Therefore, measuring the penetration fraction, resulting from the integration of the growth factor distribution, has little use in hygroscopicity studies. By assuming (instead of measuring) a total population exiting DMA1, the growth factor distribution can still be calculated. The shape of the growth factor distribution remains intact when using the assumed total population, and therefore, the growth factor results can be used to calculate hygroscopicity without the use of a DMA1 CPC.

[Figure 1]

The flat and singly-charged assumptions used by traditional inversion routines may create biases and spurious trends that confound the experimental results. The flat inlet size distribution assumes the second derivative of the inlet size distribution is equal to zero. The second derivative of a log-normal size distribution is equal to zero in only one place: the maximum. Additionally, the total population exiting DMA1 always contains some multiply charged particles. Therefore, neither the flat assumption nor the single charge assumption is exactly true, and the biases generated by the assumptions should be investigated (Swietlicki et al., 2008). When performing experiments, multiple growth factor distributions are often compared to understand how the growth factor distribution changes as a function of time (Alroe et al., 2018; Martin et al., 2013; Tritscher et al., 2011) or diameter (Carrico et al., 2010; Varutbangkul et al., 2006). Since inversion routines assume a flat inlet size distribution with every inversion, the implicit assumption in this comparison is that the inlet size distribution is constant over time. In many experiments, the inlet size distribution changes with time. Thus, the biases that are created by the inlet size distribution assumptions can create spurious trends as a function of time or diameter, and these biases and trends are likely confounded with reported conclusions.

In this study, we evaluate the impact of the inlet size distribution on the CPC response and include the inlet size distribution in the inversion process. We first show theoretically how the inlet size distribution shifts the CPC response with no change in relative humidity. This modeling exercise, using empirical relations describing the growth of ammonium sulfate, shows that multiply charged particles do not grow the same as singly-charged particles in DMA2 mobility space. This theoretical observation is then confirmed experimentally using aerosol emitted from the flaming combustion of grass. When the CPC response generated by the flaming combustion of grass is inverted, we find a single growth factor distribution describes all charges present, contradicting traditional inversion results.

2. Definitions

The neutralized size distribution entering DMA1 is called the inlet size distribution, which is assumed to be either lognormal or flat throughout this study. A flat inlet size distribution is defined as a size distribution in which the second derivative is equal to zero. DMA1 selects a small portion of the inlet size distribution, and the set of size distributions exiting DMA1 is called the selected size distributions set. Each element in the set of selected size distributions is associated with a number of charges (+1, +2, +3, etc.), and to reference this association, we use the adverbs singly-, doubly-, triply-charged, etc. Additionally, each DMA has a set of transfer functions that are specific to each of the associated charges.

Once the selected size distributions pass through the humidifier, water condenses on the particles transforming the “selected” size distributions into the “experimental” size distributions. Like the selected size distributions, we identify the elements of the experimental size distribution set using the previously mentioned adverbs.

Total population is defined as the total number of particles within a size distribution. The DMA2 CPC response results from scanning DMA2 by mobility and counting the total number of particles using the CPC. In this document, we express the DMA2 CPC response as the number of particles per cubic centimeter as a function of DMA2 mobility. The reader must recognize that the CPC counts particles irrespective of the number of charges on the particle. So, the measured DMA2 CPC response is the sum of the DMA2 CPC responses for each experimental size distribution entering DMA2. Inverting the DMA2 CPC response calculates the sum of the experimental size distributions entering DMA2. Since both the DMA2 CPC response and its inversion technically contain contributions from each of the experimental size distributions of different charges, the previously mentioned adverbs apply to the DMA2 CPC response and its inversion. As previously mentioned, the H-TDMA inversion calculates the growth factor distribution that characterizes the hygroscopic growth of the aerosol. Graphically represented, the abscissa of the growth factor distribution is the growth factor (G_f): the wet diameter (D_w) divided by the dry diameter (D_d) as shown in Equation 1. The ordinate is the derivative of the penetration fraction (F), the number of dry particles (N_d) converted to wet particles (N_w) (Equation 2), with respect to the growth factor as shown in Equation 3. These definitions are shown graphically in *Supplemental Information S1*.

$$G_f = \frac{D_w}{D_d} \quad \text{Growth Factor} \quad (1)$$

$$F = \frac{N_w}{N_d} \quad \text{Penetration Fraction} \quad (2)$$

$$\frac{dF}{dG_f} = f(G_f) \quad \text{growth factor distribution} \quad (3)$$

3. Computational Methods

Section 3 describes two computational methods: a full forward model and an inversion method. The full-forward model is used in Section 4 to investigate the role of the inlet size distribution on the CPC response. This investigation includes two case studies. The inversion method is used in Section 5 to invert experimental data. This inversion does not double deconvolve the growth factor distribution in a single step; the inversion uses a two-step process that first deconvolves the DMA2 transfer function and then deconvolves the growth factor distribution. This two-step inversion enabled reuse of sub-routines used in the full forward model.

3.1. Full forward model

To understand the influence that the inlet size distribution has on H-TDMAs, the theoretical full forward model (TAO) needs to calculate the DMA2 CPC response as a function of the inlet size distribution and DMA transfer function width. The model must be able to first calculate the selected size distributions exiting DMA1. This method should incorporate the inlet size distribution and DMA1 transfer function when calculating the selected size distributions. This calculation should include not only the inlet size distribution, but the presence of multiply charged particles. Once the influence of the inlet size distribution and of the DMA1 transfer function is incorporated in the set of selected size

distributions, the remaining calculations will carry the influence of the two variables through the remainder of the model. The model must then convolute the selected size distributions with a given growth factor distribution to create the experimental size distributions. Lastly, the model should then calculate the DMA2 CPC response using the DMA2 transfer function and experimental size distributions, keeping track of the DMA2 CPC response as a function of particle charge. Then, by changing the inlet size distribution and the DMA transfer functions, the model calculates the influence the variables have on every step in the H-TDMA process, including the final DMA2 CPC response. Any change in the DMA2 CPC response, due to a change in the inlet size distribution, would be recognized by the traditional inversion routines (excluding (Markus D Petters, 2018)) as a change in the growth factor distribution, although technically no change in growth factor distribution occurred. A general description of TAO is found below, and a detailed description and flow chart is found in *Supplemental Information 2*.

TAO incorporates the inlet size distribution (ISD) and DMA1 transfer function when calculating the selected size distributions (SSD) exiting DMA1, as shown in Equation 4 (Rader & McMurry, 1986). TAO assumes that the inlet size distribution is log normal. The DMA1 subroutine multiplies the inlet size distribution ($dN_d/d\ln(D_d)_{ISD}$) by the DMA1 transfer function (Ω_1) and the charging fraction (f_c) (described below). This process is repeated for each of the selected size distributions up to a maximum of 10 charges (m). While distributions could be referenced as either dN/dD or $dN/d\ln(D)$, for conceptual purposes, our model then converts from $dN/d\ln(D)$ to dN/dD by dividing by the particle diameter. TAO then integrates each of the selected size distributions to determine the total population of each selected size distribution. While the cutoff threshold can be user defined, for this study, any selected size distribution that contributes less than 0.1% of total particles exiting DMA1 is deleted. When specifying many charges, deletion of those charges by the routine identifies for the user which charges are unnecessary. Many relationships are used to calculate the selected size distributions exiting DMA1. The lognormal size distribution is defined by Friedlander (2000). The mean free path, viscosity of air, and Cunningham correction factor are calculated using formulas from Kim, Mulholland, Kukuck, and Pui (2005). The first two charges in the bipolar charge distribution is calculated using the empirical fits by Wiedensohler (1988) and coefficients from Baron (2005). For charges greater than 2, the relationship from Gunn (1956) is used along with assuming the published value for the ratio of electrical mobilities of positive to negative ions from Wiedensohler (1988). The non-diffusing transfer function from Knutson and Whitby (1975) is used to model the DMA1 transfer function, which is a function of voltage (V_1) and flow rates (Q_1). In this study, we limited our investigation to larger particle sizes in a TSI long DMA which can be modeled with the non-diffusing transfer function. The output from the DMA1 subroutine is the set of selected size distributions, one for each relevant charge m (+1, +2, +3, etc.) as a function of DMA1 transfer function, charging fraction, and inlet size distribution.

$$\left[\frac{dN_d}{dD_d}(D_d, m) \right]_{SSD} = \frac{\Omega_1(V_1, D_d, Q_1, m) f_c(D_d, m)}{D_d} \left[\frac{dN_d}{d\ln(D_d)}(D_d) \right]_{ISD} \quad (4)$$

The current TAO code has the capacity to model the growth of the selected size distributions using one of two methods: convolution with a growth factor distribution or assuming the aerosol is ammonium sulfate. The user specifies which of the two methods and, if necessary, provides the growth factor distribution to be used. The experimental subroutine uses this information along with the selected size distributions from Equation 4 to calculate the experimental size distributions. As shown in Figure S4, the subroutine begins by integrating each of the selected size distributions, which converts from dN/dD space

to $N(D)$ space. For ammonium sulfate, which is used in the case studies below, the user enters a relative humidity, and the experimental routine uses the selected size distribution (dry) diameter, the activity of water Tang and Munkelwitz (1994), and the Kelvin effect to iterate for the correct ammonium sulfate growth factor. In this case, the ammonium sulfate growth factor is then multiplied by the dry diameter to determine the wet diameter. The population at each diameter remains unaffected by the growth as shown by Equation 5. This process is performed for each selected size distributions, one for each charge (m) (+1; +2; +3; etc.). The final step is to calculate the experimental size distribution (dN_w/dD_w) from $N_w(D_w)$. To understand how TAO handles growth factor distributions, see *Supplemental Information S2.5*. The output from this step is the set of experimental size distributions as a function of inlet size distribution, DMA1 transfer function, charging fraction, and growth method.

$$[N_w(D_{d,i}G_{f,as}, m)]_{EXP} = [N_d(D_{d,i}, m)]_{SSD} \quad \text{ammonium sulfate} \quad (5)$$

The desired final DMA2 CPC response is calculated using the non-diffusing transfer function (Knutson & Whitby, 1975). Since the model treats each experimental size distribution independently, the integration is individually performed on all experimental size distributions (each charge m), and the reported DMA2 CPC response is the sum of all integrations as shown in Equation 7. The DMA2 subroutine again uses all relationships used previously by DMA1. No particle loss function or CPC detection efficiency is used in this model. The output from this step is the DMA2 CPC response, at every DMA2 setpoint (n), as a function of inlet size distribution, DMA1 transfer function, charging fraction, growth method, and DMA2 transfer function. Any change in the DMA2 CPC response created by the inlet size distribution in the model displays the phenomena that is missing in traditional inversion routines. The definition of the derivative of wet diameter with respect to particle mobility can be found in *Supplemental Information S2.3*.

$$N_{CPC,n} = \sum_{m=1}^{nc} \frac{Q_{2,a}}{Q_{2,s}} \int_{\tilde{z}_{p,0,m}}^{\tilde{z}_{p,f,m}} \Omega_2 \frac{dN_{w,m}}{d(D_w)} \frac{d(D_w)}{d\tilde{z}_p} d\tilde{z}_p \quad (7)$$

3.2. Inversion of experimental results

We created a new inversion routine (named Junior) to invert the experimental results in section 5 below. This inversion routine has the option to either include or neglect the inlet size distribution during inversion, which enables assessment of the impact of Slope and Multi-Charge Dispersion (MCD) bias (see section 4 below). When neglecting the inlet size distribution, the routine assumes the inlet size distribution is flat in the area of the DMA1 transfer function and only the singly-charged selected size distribution exists. This mode simulates traditional inversion routines. When including the inlet size distribution, both the Slope bias and MCD bias are considered. This choice moves beyond Markus D Petters (2018), which accounts for Slope bias, by accounting for MCD bias. Additionally, the routine can invert the CPC response for an individual charge. Lastly, the routines used in the forward model above (TAO) were reused when possible. A flow chart, as well as additional descriptions on the use of Junior, can be found in *Supplemental Information S4*.

The Junior inversion routine does not perform the double deconvolution in a single step. Instead, Junior deconvolves the DMA2 transfer function from the CPC response first (the integration over wet diameter), and then deconvolves the growth factor distribution in a separate second step (the integration over dry diameter). The result of the first deconvolution is the experimental size distribution entering DMA2, and the determined experimental size distribution is the sum of all charges present. The second deconvolution calculates the growth factor distribution for all charges considered. This two-step process allowed the quick use of the routines written for the forward model above. In both steps, the routine assumes that a number of statistical distributions describe the shape and population of the objective distribution and is necessary as the problem is ill-posed. As shown in *Supplemental Information S5*, when an incorrect statistical distribution shape is assumed, error can occur. However, this error is small in comparison to the error generated when neglecting the inlet size distribution. Thus, this inversion is sufficient to compare inclusion to neglect of the inlet size distribution during the inversion process. For the role of CPC noise on inversion, see *Supplemental Information S6*.

In the first step, the routine minimizes the objective function shown in Equation 8. In Equation 8, $R_{CPC,n}$ is the measured CPC response at the n^{th} DMA2 voltage; $N_{CPC,n}$ is the calculated number of particles detected by the CPC; and γ is a regularization multiplier, which is a function of the measured CPC response divided by the maximum measured CPC response (the $R_{CPC,n}$ fraction). A range of multiplier values were manually selected specific to our data (See Table 1). These values are adjustable by the user, and in this study, the values were never adjusted. The purpose of the multiplier is to penalize errors at smaller CPC concentrations that would otherwise be treated the same as identical errors at higher CPC concentrations.

$$dist. variables = argmin \left\{ \sum_n \gamma \left(\frac{R_{CPC,n}}{maximum(R_{CPC})} \right) [R_{CPC,n} - N_{CPC,n}]^2 \right\} \quad (8)$$

[Table 1]

To minimize Equation 8, the routine assumes a set of distribution variables (*dist. variables*) defining a statistical distribution (or set of statistical distributions). This statistical distribution (or set of distributions) represents the experimental size distribution entering DMA2, as shown in Equation 9. In Equation 9, *dist. variables* are the variables defining the assumed statistical distribution(s), and p is the number of assumed statistical distributions. For this step, the routine assumes that only singly charged particles are present in the distribution. The available distributions are gaussian, beta, or log-normal distributions, and the user can use multiple distributions of one type, as necessary. In this study, beta distributions are used throughout and has been found useful in nearly all instances.

$$\left[\frac{dN_w}{dD_w}(D_w, 1) \right]_{EXP} = \sum_p \left[\frac{dN_w}{dD_w}(D_{w,p}, 1, dist. variables) \right]_{EXP,p} \quad (9)$$

The routine uses these statistical distributions to calculate $N_{CPC,n}$ using Equation 10 below, and the calculated $N_{CPC,n}$ from Equation 10 is substituted into Equation 8 above. No CPC loss function is used in the routine. The minimization in Equation 8 is accomplished using the *lsqnonlin* routine in MATLAB. The output from the routine contains the variables describing the assumed distribution and population (the experimental size distribution) entering DMA2. It is important to note that throughout this work, we used

two distributions (bimodal) to describe the measured experimental size distributions found in section 5 below.

$$N_{CPC,m} = \int \Omega_2(V_n, D_w, Q_2, 1) \frac{Q_{2,a}}{Q_{2,s}} \left[\frac{dN_w}{dD_w}(D_w, 1) \right]_{EXP} dD_w \quad (10)$$

The output of the first step, the experimental size distribution entering DMA2, is used in the second step to calculate the growth factor distribution that transforms the selected size distributions exiting DMA1 into the solved experimental size distribution. In this second step, the routine minimizes the objective function shown in Equation 11. In Equation 11, γ is again the regularization multiplier which assumes the values and methods as described in the previous step. N_w is the absolute number of particles (for all charges present), in bin k , in the experimental size distribution output from the first step above. F is the growth factor distribution, and N_d represents the dry particle distribution. All are explained further below.

$$F \text{ dist. variables} = \operatorname{argmin} \left\{ \sum_k \gamma \left(\frac{N_w(k)}{\operatorname{maximum}(N_w)} \right) (FN_d(k) - N_w(k))^2 \right\} \quad (11)$$

The number of particles in bin k is calculated by integrating the experimental size distribution, obtained by step 1, using mobilities Z_q and Z_{q+1} as limits, as shown in Equation 12. In Equation 12, q represents the mobilities at DMA2 conditions assuming the experimental size distribution is singly charged. Although the experimental size distribution and the Equation 12 integral assume a single charge, the result of the integration will be the total number of particles in the bin, irrespective of charge, as will be seen below.

$$N_w(k) = \int_{Z_q}^{Z_{q+1}} \left[\frac{dN_w}{dD_w}(Z_q, \text{dist. variables}) \right]_{EXP} \frac{dD_w}{dZ_q} dZ_q \quad (12)$$

The growth factor distribution, in Equation 11, is expressed as $F(g_f)$ (not dF/dg_f) and, like step 1, is defined by assumed statistical distributions, where p is again the number of assumed distributions, as shown in by Equation 13. In Equation 13, $F \text{ dist. variables}$ is the distribution variables defining the growth factor distributions.

$$F(j) = \sum_p \left[\int_{j-1}^j \frac{dF}{dg_f}(F \text{ dist. variables}) dg_f \right]_p \quad (13)$$

The two-dimensional dry array (N_d), in Equation 11, is calculated using the integral shown below in Equation 14. The selected size distribution inside the integral is defined by Equation 4 above. This integration is performed for each charge m , each growth factor j , and each bin k . The outcome of this integral is the number of dry particles that correspond to bin k of wet particles given the growth factor j and charge m .

$$N_d(k, j, m) = \int_{Z_s}^{Z_{s+1}} \left[\frac{dN_d}{dD_d}(Z_s, m) \right]_{SSD} \frac{dD_d}{dZ_s} dZ_s \quad (14)$$

The limits for the Equation 14 integral are defined by Equation 15. In Equation 15, s represents conditions in DMA1. Each wet diameter limit, defined by q conditions above, has a dry diameter limit, at s conditions, given a growth factor j and charge m . The discretization of Equation 4 does not perfectly match the limits calculated by Equation 15. When the limits are between discretized diameters, linearity between points in the selected size distribution is assumed.

$$Z_s = \frac{m e C \left(\frac{D_{w,q}}{g_{f,j}} \right)}{3 \pi \mu \left(\frac{D_{w,q}}{g_{f,j}} \right)} \quad (15)$$

The minimization, in Equation 11, is again accomplished using the *lsqnonlin* routine in MATLAB. The output from the second step is the variables describing the statistical distributions (*F dist. variables*), which represent the growth factor distribution. Again, we used two distributions (bimodal) in all experiments in section 5.0 below to describe the growth factor distribution.

4. Theory: The Influence of the Inlet Size Distribution

Here, we investigate the impact of the influence of the inlet size distribution on the CPC response. We first investigate the flat size distribution assumption, and then follow that analysis with the single charge assumption. For both cases, we assume two example inlet size distributions, and hold all H-TDMA settings constant. When evaluating the flat inlet size distribution assumption, no growth is assumed, and the selected size distributions are passed directly to the DMA2 subroutine for integration. For the single charge assumption, we assume the aerosol is ammonium sulfate at 90% relative humidity. We finish by showing how the biases can create spurious trends by first using one of the example size distributions, and then by using a changing inlet size distribution measured during an independent study.

4.1. Slope bias caused by the flat inlet size distribution assumption

The slope of the inlet size distribution, when crossing the DMA1 transfer function, alters the shape of the selected size distribution as shown in Figure 2 (DMA1 set to select 100 nm particles in this example). In panel (a), the orange line represents the flat inlet size distribution assumption used in inversion routines. Consider initially that the blue size distribution is the actual inlet size distribution. The dependent variable (population) of the blue inlet size distribution is higher than the flat inlet size distribution (more particles) on the left side of the DMA1 transfer function as shown by the blue arrow. On the right side of the DMA1 transfer function, the blue inlet size distribution is below the flat inlet size distribution (less particles). When the example inlet size distributions are multiplied by the DMA1 transfer function (Equation 4), this trend becomes part of the selected size distribution as shown in panel (b). The blue selected population on the left side of the DMA1 centroid is higher than the flat selected population, and the blue selected population on the right side is lower. This pattern is reversed when assuming the red size distribution.

[Figure 2]

Unfortunately, inversion routines interpret the altered population as a shift in diameter. Figure 2(c) displays the integrated DMA2 CPC response from the selected size distribution in Figure 2(b). Like the

selected size distribution, the integrated signal from the DMA2 CPC response displays a vertical shift in population. The vertical shift in the population causes an apparent left-right shift in DMA2 CPC response (Rader & McMurry, 1986). When the slope of the inlet size distribution is negative, with respect to diameter, the DMA2 CPC response shifts to smaller diameters. Positively sloped inlet size distributions shift the DMA2 CPC response to larger diameters. We refer to the impact of the slope of the inlet size distribution on the DMA2 CPC response as Slope bias throughout the remainder of the document. A negative slope in the area of the transfer function generates a negative Slope bias, and a positive slope generates a positive Slope bias.

Two more observations about Slope bias should be pointed out. First, the greater the deviation from the flat inlet size distribution assumption, the stronger the Slope bias. If, for example, we widen the DMA1 transfer function at the same centroid location, the deviation from the flat inlet size distribution increases, and Slope bias increases. Second, if the particles experience growth, the diameter at the peak of the DMA2 CPC response will be the growth factor multiplied by the shifted diameter interpreted by DMA2 above. The shift in diameter in Figure 2(c) is how DMA2 interprets the selected size distribution without growth. If these particles experience growth, their growth begins at the diameters shown in Figure 2(c), not the DMA1 centroid. Thus, the final wet size is a combination of the growth factor and the Slope bias. We note that the inversion routine created by Markus D Petters (2018) takes Slope bias into consideration during inversions.

4.2. Multicharge Dispersion bias caused by the single charge assumption

Figure 3 adds the doubly- and triply-charged DMA1 transfer functions to Figure 2. Instead of plotting the value of the transfer functions on the alternate y-ordinate as in panel (a), the product of the transfer function and the charging fraction is plotted. Only the Slope bias for the singly-charged transfer function was considered above; In Figure 3, each selected size distribution has its own Slope bias. For the blue inlet size distribution, the slope in the area of all three transfer functions is negative; and the net Slope bias will be negative. For the red size distribution, the inlet size distribution has a positive slope at the singly-charged transfer function, has a near neutral slope at the doubly-charged transfer function, and a negative slope at the triply-charged transfer function. The net Slope bias for any situation will depend on the total population of each selected size distribution as well as its Slope bias. The singly-charged selected size distribution from the blue inlet size distribution constitutes 93% of the selected size distribution total population. Thus, the negative Slope bias associated with the singly-charged selected size distribution is a good estimate of the overall negative Slope bias from the blue inlet size distribution. The singly-charged selected size distribution resulting from the red inlet size distribution contains only 55% of the total population. The doubly- and triply-charged selected size distributions are significant contributors to the net Slope bias. The population of the red inlet size distribution, at the location of the doubly- and triply-charged transfer functions, is much higher than the blue inlet size distribution, and this difference in population alters the total population of the selected size distributions. This change in total population alters the net Slope bias and can create significant Multicharge Dispersion (MCD) bias defined below. Additionally, when sampling different DMA1 diameters, the charging fraction can change significantly. The change in charging fraction also changes the total populations of the selected size distributions.

[Figure 3]

When all elements of the selected size distributions experience the same growth factor, they grow unequally in single charge diameter space, making a non-monodisperse response (Gysel et al., 2009). For example, we assume a singly-charged 100 nm particle shown in Table 2 (centroid of Figure 3 DMA1 transfer function). The corresponding doubly- and triply-charged sizes are 151.1 and 195.4 nm respectively. We assume that all three particle sizes experience a growth factor of 1.7. As expected, the

singly-charged particle has a growth factor of 1.7, however, the doubly-charged and triply-charged particles have smaller apparent growth factors in single charge diameter space (as would be measured by DMA2 CPC). If the doubly- and triply-charged selected total populations are large, as in the red size distribution, the selected total population does not grow like a monodisperse total population. In contrast, the blue inlet size distribution creates a mostly singly-charged selected total population. Thus, this selected total population for the blue inlet size distribution grows as if it is monodisperse. MCD bias occurs when the selected total population does not act as a monodisperse total population. As the growth factor increases, the inequivalent growth in single charge diameter space increases, and the potential for MCD bias increases. At low growth factors (less than 1.1), the MCD bias is minimal, and the response behaves as a monodisperse aerosol, even if multicharged.

[Table 2]

In Figure 4, we have assumed that the selected size distributions, from Figure 3, are ammonium sulfate, and the H-TDMA conditioner elevated the relative humidity to 90%. Under those conditions, a 100 nm particle should grow by a growth factor of approximately 1.7. The total DMA2 CPC response and the contributions to that response from the first three charges are shown. The blue size distribution is primarily singly charged, and the total response matches well with the singly-charged experimental size distribution (monodisperse). The peak of the response is less than the nominal 170 nm. The Slope bias for the singly-charged selected size distribution is negative, and this bias generates the lower DMA2 CPC response peak. For the red size distribution, the biases are different. The singly-charged selected size distribution is under positive Slope bias, and the apparent growth factor for the singly-charged experimental size distribution is greater than 1.7. However, the doubly- and triply-charged selected size distributions are under neutral and negative Slope bias respectively. Additionally, the total population behaves as a disperse total population, and the MCD bias decreases the apparent growth factor. The two biases combine to create a lower than nominal growth factor. The peak of the response in both panels is near 168.5 nm, and this similarity and small bias may not cause alarm, however, we explore cases below where spurious trends can emerge.

[Figure 4]

4.3. Spurious trends created by the two biases

For the first case study, we assume the red inlet size distribution is static, and we compare the DMA2 CPC response for different DMA1 set points. Again, we assume the growth of ammonium sulfate aerosol after increasing the relative humidity to 90%. The peak of the DMA2 CPC response, which is very close to the actual inverted peak location, is compared to the ideal response calculated using the DMA1 centroid and the relationships from Tang and Munkelwitz (1994). The hygroscopicity for both the ideal response and the peak location are used to calculate the percent error. These results are shown in Figure 5(a).

[Figure 5]

Although the response is complicated, the net bias generates an apparent decrease in hygroscopicity as selected particle diameter increases. When the aerosol-to-sheath ratio of DMA1 is changed from 1:10 to 1:4, the percent error in hygroscopicity is amplified. The Slope bias is the primary cause of the amplified error. In general, the slope of the inlet size distribution moves from positive to negative as the diameter increases. Additionally, the width of the DMA1 transfer function increases with an increase in set point diameter, which as previously mentioned increases the Slope bias. When the aerosol-to-sheath ratio is 1:10, the DMA1 transfer function is narrow, and Slope bias is significantly reduced. However, this choice of aerosol-to-sheath ratio does create a more complicated response. At 50 nm, the total population is

significantly multiply charged, and the net bias is negative. This negative bias decreases for 100 nm and then stabilizes once the initial size is greater than the peak of the inlet size distribution. When sampling on the right side of the inlet size distribution, the sampled total population is mostly singly charged, but the Slope bias is negative.

Additionally, the data in Figure 5(a) assumes a constant aerosol-to-sheath ratio, but this is likely not reality. For example, we assume an aerosol flow of 1.5 lpm. A sheath flow rate of 15 lpm (aerosol-to-sheath ratio of 1:10) can sample diameters up to 200 nm for the physical voltage and column length limitations of a TSI long DMA design. The sheath flow would need to be slowed to sample larger diameters; thus, a wider transfer function would need to be used. This wider transfer function would increase the Slope bias (like the 1:4 example in panel (a)) and increase the negative net bias. This modeling experiment is similar to observing the changes in hygroscopicity or growth as a function of dry diameter. In the Carrico et al. (2010) study, the growth factor was large and the aerosol-to-sheath ratio was 1:5 in the experiment. An overall loss in hygroscopicity with an increase in dry diameter was observed for all biomass fuels tested. In the Varutbangkul et al. (2006) study, the growth factor was low, and an overall loss in growth was sometimes observed with larger diameters. The results of this modeling study do not specifically alter these two chosen example studies, and the two examples have other factors specifically influencing growth factor; however, the published results could be confounded with these biases and trends resulting from the inversion routine assumptions.

For the second case study (Figure 5(b)), we assume an experimental chamber is used. We use a previously measured inlet size distribution, created from the flaming combustion of 15 g grass, evolving in a 21 m³ experimental chamber over a two-hour time period. During this time period, the particles in the experimental chamber deposit on the walls and agglomerate with one another, and the emitted gases condense on the existing particles and walls (Nah, McVay, Pierce, Seinfeld, & Ng, 2017). DMA1 is assumed static at 150 nm, and we assume the growth of ammonium sulfate aerosol when relative humidity is elevated to 90%. The mean of the inlet size distribution begins at a diameter smaller than the centroid of the transfer function and quickly becomes larger. Although the Slope bias changes throughout the experiment, MCD bias is the major contributor to the changes in panel (b). The fraction of multiply charged particles increases over the course of the experiment, and this increase creates the apparent loss in hygroscopicity as a function of time. If the growth factor was much less (less than 1.1), then the Slope bias would dominate, and the hygroscopicity error would increase as a function of time. For large growth aerosols, the net bias in chamber experiments creates an apparent loss in hygroscopicity. For small growth aerosols, the net bias in chamber experiments creates an apparent increase in hygroscopicity. This example is like many chamber and oxidation experiments. In the Alroe et al. (2018) and Martin et al. (2013) studies, a high growth aerosol decreased in hygroscopicity as a function of time in the chamber. In Tritscher et al. (2011), a low growth aerosol increased in hygroscopicity as a function of time in the chamber. Again, the outcome of this modeling study does not alter the previously published results as there are other factors also influencing growth factor, for example the evolution of aerosol chemical composition. However, in all three cases, the results of the published studies could be confounded with the biases and trends resulting from the inversion routine assumptions.

This study highlights that in certain experimental conditions spurious hygroscopic trends, with respect to diameter and experiment time, can occur when not considering the inlet size distribution. These theoretical trends are a function of DMA1 diameter, the shape of the inlet size distribution, the growth factor distribution, and the DMA1 aerosol-to-sheath ratio. When not including the inlet size distribution, these variables, and the interactions between these variables, create a complicated response that includes

the interaction between the two biases defined above. This situation makes prediction of the trends difficult without the help of a theoretical model or proper inversion routine.

5. Experimental Measurement of MCD Bias

5.1. Experimental setup

MCD bias occurs when the growth of the aerosol, in DMA2 mobility space, is unequal between the charges. This unequal growth has never been experimentally confirmed to our knowledge. To observe this phenomenon, a high growth aerosol must be chosen, and the CPC response must be attributed to each of the individual charges. If MCD bias is true, under these conditions, the CPC response for each charge should differentiate by DMA2 mobility as shown in Figure 4(b). Measurement of this phenomenon is the goal of this methods section.

A small amount (5 g) of grass from Western Montana was burned in the flaming phase in a 21 m³ environmental chamber. A minimal amount of iso-propanol was used to start the combustion process, and this burning iso-propanol ensured the grass was engulfed in flame and quickly consumed. The emitted aerosol, from the chamber, passed through a pre-humidifier reaching humidities in excess of 90%, and then, the particles were dried to below 15% relative humidity as shown in Figure 6. The pre-humidification process was intended to collapse agglomerates (Lewis et al., 2009) in order to adhere to the spherical particle assumption required by DMAs. The dry particles passed over 2 polonium-210 neutralizer strips (2xNRD 2U500) in a Particle Technology Laboratory casing. The neutralized sample flow was then split: 0.3 LPM of the aerosol sample fed a TSI 3696 Scanning Mobility Particle Sizer (SMPS) and 1.5 LPM of aerosol entered the TDMA (Oxford et al., 2019). DMA1 was set to 120 nm throughout the experiment. This size was intended to ensure multi-charging would occur to various degrees throughout the experiment. The selected size distributions passed through a pair of Nafion membranes to achieve 90% relative humidity. The second DMA measured the experimental size distributions in two different ways. 1) stepping voltages when feeding particles directly to the DMA2 CPC, known further as TDMA mode and 2) static voltage when feeding particles to the Centrifugal Particle Mass Analyzer (CPMA)(Olfert & Collings, 2005), known further as CPMA mode. When directed to the CPMA, the aerosol was returned to DMA1 conditions using a set of silica driers. The CPMA then scanned the dried aerosol to determine the fraction of the DMA2 CPC response attributed to each charge.

[Figure 6]

Throughout the experiments, an SMPS measured the inlet size distribution. All measured inlet size distributions were fully described by a single log-normal size distribution. While the SMPS measured the inlet size distribution, the TDMA/CPMA operated in the two modes as mentioned above. In each experiment, the TDMA completed a single scan in TDMA mode at both the beginning and the end of the experiment. The TDMA scans shown in this study were taken at 6 minutes and 2.5 hours after the burn. In the interim, we ran the instrument in CPMA mode. We set DMA2 to a fixed diameter, and the CPMA was scanned. The process of setting a DMA2 diameter and scanning the CPMA was repeated for 15 different DMA2 diameters. The order of the diameters was alternated between different sides (by diameter) of the maximum of the DMA2 CPC response. For example, a CPMA mode scan would measure a 130 nm DMA2 setting, then the DMA2 centroid would be moved to 250 nm, and another measurement taken (peak of DMA2 CPC response ~215 nm). If any time related biases, caused by the

changing inlet size distribution, occurred, the bias would appear as alternating between DMA2 set points. An example of the CPMA measurement is shown in Figure 7(b).

[Figure 7]

The CPMA mode mass size distributions allocated the DMA2 CPC response to one of the first three charges. Most of the CPMA CPC responses split into the three separate curves, one curve for each charge. However, at smaller growth factors, the responses overlapped. We inverted the CPMA response using non-diffusing transfer functions defined by Olfert and Collings (2005). After inversion, we assumed that a single beta distribution represented each charge, and the start and stop of the distribution were defined by the limits of the DMA1 transfer function. The beta distribution shape factors and population were iterated, along with the particle density to determine the mass size distribution. The optimization function used was a simple sum of the squares of the error between the CPMA CPC response and the calculated CPC response. We summed the total particle count from each distribution and calculated the number fraction using the sum. The fraction was then multiplied by the total DMA2 CPC measurement as shown in panel (a). In this example, of the 100 particles sampled by the DMA2 CPC, 84 were due to the first charge, 15 for the second, and 1 for the third. The method shown in Figure 7 encapsulates the concept, but the process is more complicated, due to the changing inlet size distribution.

Each of the 15 CPMA mode scans took 9 minutes to complete, and the 15 CPMA mode scans took over two hours. Over that period, the total chamber population decreased to 19% of the original population. Thus, if the final CPMA scan were performed at the beginning of the experiment, the total number of particles measured would be significantly more. This particle loss in the chamber biases the CPMA measurements as a function of time. Additionally, the TDMA scans occur at different times than each of the CPMA scans. Thus, each CPMA measurement must be corrected for the change in population in the experimental chamber. The first step in the correction process is to normalize the integrated CPMA particle count, from Figure 7(b) using the theoretical total population exiting DMA1 at the time of measurement. This normalized CPMA value was then multiplied by the theoretical total population exiting DMA1 at the time of the TDMA scan of interest. After correction for the changing population, the fraction attributed to each charge could then be calculated at the time of the TDMA scan. Unfortunately, the diameters chosen for the CPMA scans do not align with the diameters selected for the TDMA scans. Thus, three polynomials, one for each charge, were fit to all fractions as a function of DMA2 mobility to create a continuous function at the time of interest. These three polynomials were used to determine the final fractions that were multiplied by the CPC count as shown in Figure 7(a). See *Supplemental Information S3* for a more specific description of the correction process and a plot of the polynomials.

5.2. Experimental results

The DMA2 CPC response for each charge does not align in mobility space as seen in Figure 8(a). The overall DMA2 CPC response data comes from the final TDMA mode scan 2.5 hours after the burn. The polynomials, developed using the CPMA mode and SMPS scans during the experiment, apportion the DMA2 CPC response to each of the first three charges. The DMA2 CPC data clearly display the misalignment theoretically proposed in Table 2: the first charge apparently grows more than the second, which apparently grows more than the third. The reader must remember that the doubly- and triply-charged CPC responses do not actually have the physical diameter shown on the abscissa.

[Figure 8]

In creating Figure 8(a), we have assumed that the population of quadruply and larger charged particles are equal to zero. Thus, only the first three charges are assumed present. Measurements of charges greater than three were possible in some instances (lower growth factors) but were often difficult. The triply-charged response was quantifiable through most of the range. However, at higher DMA2 mobilities (approximately 120 to 170 nm assuming singly charged), the CPMA mass size distributions for the first three charges overlapped with low CPC counts, when combined resulted in noisy multi-charge inversions. Above 170nm (Figure 7b), the three distributions were mostly deconvolved with high CPC counts making inversion accurate.

Each CPC response, for the three charges presented in Figure 8(a), is inverted individually by Junior (section 3.2) considering both the Slope and MCD biases. These inversion results are shown by the colored dotted lines in Figure 8(b). Additionally, the inversion, assuming the inlet size distribution is flat and the selected size distribution is singly charged, is shown as the black dashed line. The overall penetration fraction of the first three charges ranges from 0.54 to 0.67. The overall penetration fraction for the flat and singly-charged assumption is 1.31. This physically impossible penetration fraction is due to the singly-charged assumption. The Pearson correlation between the cumulative growth factor distributions for the first three charges agree better with one another (0.992 to 0.998) than with the cumulative growth factor distribution that assumes that the inlet size distribution is flat and that the selected size distribution is singly charged (0.983 to 0.996). Thus, values and shapes of the growth factor distributions for the individual charges (Figure 8b) are more similar to one another than they are with the flat and singly-charged inversion.

Since the growth factor distributions for first three charges are quite similar, one may assume that a single growth factor distribution describes all three of the evaluated charges. This inversion is shown as the solid black line in Figure 8(b). When comparing the cumulative growth factor distributions, the correlation between the measured charges and the single growth factor distribution assumption is 0.996 to 0.998, which is greater than the correlation with the flat and singly-charged assumption. Additionally, this single growth factor assumption does well in explaining the measured CPC responses as shown by the colored lines in Figure 8(a). The measured CPC responses in Figure 8(a) clearly display that the singly-charged assumption is valid only for the singly-charged CPC response (green circles). The overall CPC response requires the including charges greater than 1.

The single growth factor distribution assumption contrasts previously published results showing growth factor distributions changes as a function of DMA1 diameter (Martin et al., 2013). Carrico et al. (2010) investigated many biomass fuels, including grass, during the FLAME experiments. Three diameters were selected by DMA1: 50 nm, 100 nm, and 250 nm. In general, high growth aerosols displayed bimodal growth factors at 50 nm with the upper mode growth factor sometimes approaching 1.9. The growth was attributed to the presence of inorganic material, specifically potassium and chloride. At 100 nm and especially 250 nm, the upper mode growth factor decreased. These observations suggest that growth factor is a function of diameter. Since the diameters investigated in the FLAME studies detected differences between 50 nm, 100 nm, and 250 nm, the change in growth factor could be significant enough to cause problems for the single growth factor assumption proposed above, which technically investigated DMA1 diameters from 120 nm (singly charged) through 241 nm (triply charged).

It is possible that the emitted aerosol in this study is significantly different (by composition, growth factor shape, and growth factor magnitude, etc.) than the aerosols measured in the FLAME experiments, but our results are very similar to many of the FLAME measurements. Like the FLAME

experiments (Levin et al., 2010), we detected high amounts of potassium in the emitted aerosol (*Supplemental Figure S16*), and the measured growth factors are in excess of 1.9. These growth factors are of the same order as potassium containing species (KCl, KNO₃) (Carrico et al., 2010; Kelly, Wexler, Chan, & Chan, 2008). We also, as shown in Figure 8(b), detected a bimodal growth factor distribution. Thus, the aerosol emitted in this study is quite similar to the Carrico et al. (2010) study. Additionally, the diameters measured in Figure 8(a) are similar in size to the measurements made in Carrico et al. (2010). However, we did not detect a decrease in hygroscopicity as a function of size. The growth factor distribution in this study appears to be independent of size over the range of 120 nm to 241 nm. The experimental measurements of the two aerosols are quite similar, but the experimental inversions, and thus the interpretation, are quite different.

If the aerosol in our study is comparable to the aerosol in the Carrico et al. (2010) study, then the difference between the two outcomes could be the assumptions made when inverting the data. The aerosol in our study appears to adhere to a single growth factor distribution assumption, and this growth factor distribution causes MCD bias when assuming the response is singly charged. If we were to sample the aerosol at 120 nm and 241 nm, assuming that the peak of the inlet size distribution is smaller than both sampled diameters and all particles adhere to the single growth factor distribution, then the theoretical response from the above system, when assuming the particles are singly charged, would display a loss in hygroscopicity with increasing DMA1 diameter (see Figure 5(a)). Then, the growth observations from this experiment would match the observations in the FLAME studies. Thus, making the single charge assumption without correcting for Slope bias generates a false diameter dependency which can lead to an incorrect experimental interpretation. In this experiment, the single growth factor distribution is correct. Unfortunately, there is not enough experimental information in either study to confirm this root cause creates the diameter dependence found by Carrico et al. (2010).

6. Conclusions

This work suggests that the two traditional H-TDMA inversion assumptions can create false experimental interpretations under specific conditions. Traditional inversion routines assume the inlet size distribution is flat over the width of the DMA1 transfer function, and the particles exiting DMA1 are singly charged. The combination of these two assumptions conveniently allows H-TDMA data inversion without input of the inlet size distribution. When inverting hygroscopicity data derived from aerosol emitted from the flaming combustion of grass, for example, the traditional inversion routines calculate an apparent decrease in hygroscopicity with an increase in DMA1 diameter. In contrast, when measuring the CPC responses for each charge and inverting them using a new inversion routine named Junior, the different diameters exhibit similar hygroscopic growth factor distributions. Junior uses no single charge assumption and makes no flat inlet size distribution assumption. Each charge's CPC responses and the inlet size distribution are measured quantities. Junior's inversion results contradict the traditional inversion results, and thus, the traditional inversion assumptions may lead to a false diameter dependency on observed particle hygroscopicity.

The inlet size distribution can cause false hygroscopic trends when the inlet size distribution shifts the CPC response with no change in relative humidity. Using a model named TAO, we showed that two biases, generated by the inlet size distribution, work together to shift the CPC response. Slope bias occurs when the slope of the inlet size distribution, in the area of the DMA1 transfer function, is non-zero. MCD bias occurs when each charge's size distribution appears to grow unequally, according to DMA2. These two interacting biases reinforce or cancel out shifts in the CPC response depending on instrument settings

and aerosol properties. When TAO calculated the CPC responses for ammonium sulfate at different DMA1 diameters, the CPC responses shifted to smaller DMA2 diameters with respect to increases in DMA1 diameter, although no change in relative humidity occurred. When TAO calculated the CPC responses from an ammonium sulfate size distribution evolving in a chamber, the CPC responses shifted to smaller diameters over time, although no change in relative humidity occurred. Thus, the inlet size distribution shifted the CPC responses as a function of both DMA1 diameter and experimental time. When the inlet size distribution is neglected during inversion, false dependencies in both experimental time and diameter can occur.

H-TDMA inversions should be crafted to correct for the inlet size distribution biases. To remove Slope bias, the population as a function of diameter in the area of the DMA1 transfer function, must be included in the calculations. To remove MCD bias, a multi-charge inversion must quantify the number of multi-charge particles present and must assume a hygroscopic transformation describing the growth of all charges present. In the grass combustion experiment, an estimate of the multi-charge particle population was made when including the inlet size distribution population during Junior's inversion, and all charges could be described by the same growth factor distribution.

Including the inlet size distribution during inversion, which reduces Slope and MCD bias, will enable more accurate H-TDMA inversions regardless of specific experimental conditions. Such inversions would provide proper hygroscopic dependencies with respect to diameter and experimental time, and these dependencies would enable more accurate estimates of cloud droplet numbers, which are a primary parameter influencing the Earth's climate system.

7. Acknowledgements

The modeling code created here is named in memory of CRO's mother, Theresa Ann Oxford (1948-2004). CRO and BJW acknowledge funding, in support of this work, from NSF CAREER Award number 1554061 and US EPA STAR grant number R835402. RKC gratefully acknowledges support from the US National Science Foundation (AGS-1455215 and AGS-1926817) and the U.S. Department of Energy's Atmospheric System Research program (DE-SC0021011)

8. Competing Interests

The authors declare no competing interests.

9. Nomenclature and Units

CPC – condensation particle counter. Subscript used to denote at CPC.

D_w – wet particle diameter

D_d – dry particle diameter

D – particle diameter

dist. variables – The set of variables required to define a certain statistical distribution. These variables are used to define the experimental size distribution entering DMA2

DMA1 – first differential mobility analyzer in the Tandem Differential Mobility Analyzer

DMA2 – second differential mobility analyzer in the Tandem Differential Mobility Analyzer.

EXP – experimental size distribution. Subscript used to denote after growth experiment.

F – penetration fraction. The ration of the total number of wet particles divided by the total number of dry particles.

F dist. variables – The set of variables defining required to define a certain statistical distribution. These variables are used to define the growth factor distribution that transforms the selected size distributions into the experimental size distribution.

$dF/dG_f(G_j)$ – growth factor distribution as a function of growth factor

G_f – growth factor

guess – estimate of the selected total population exiting DMA1

ISD – inlet size distribution. Subscript used to denote neutralized size distribution entering DMA1.

i – each dry diameter bin

j – each growth factor

k – each wet diameter or wet diameter bin

M – mass of the particles

m – number of charges on the particles

n – each DMA2 voltage

N – number of inlet size distribution particles

N_w – number of wet particles

N_d – number of dry particles

Q_1 – DMA1 flowrates which includes aerosol and sheath flow rates

Q_2 – DMA2 flowrates which includes aerosol and sheath flow rates

Q_a – aerosol flowrate

Q_s – sheath flowrate

q – integration limits for bin k

R_{CPC} – measured CPC response

RH_{exit} – relative humidity at the exit of the unit

SSD - selected size distribution. Subscript used to denote size distribution exiting DMA1.

V_1 – DMA1 voltage

Z – DMA2 mobility

γ – regularization multiplier

κ – measured hygroscopicity

κ_T – theoretical hygroscopicity based on Tang and Munkelwitz (1994)

μ - mean of the log-normal inlet size distribution

σ – standard deviation of the log-normal inlet size distribution

Ω_1 – DMA1 transfer function

Ω_2 – DMA2 transfer function

10. Figures

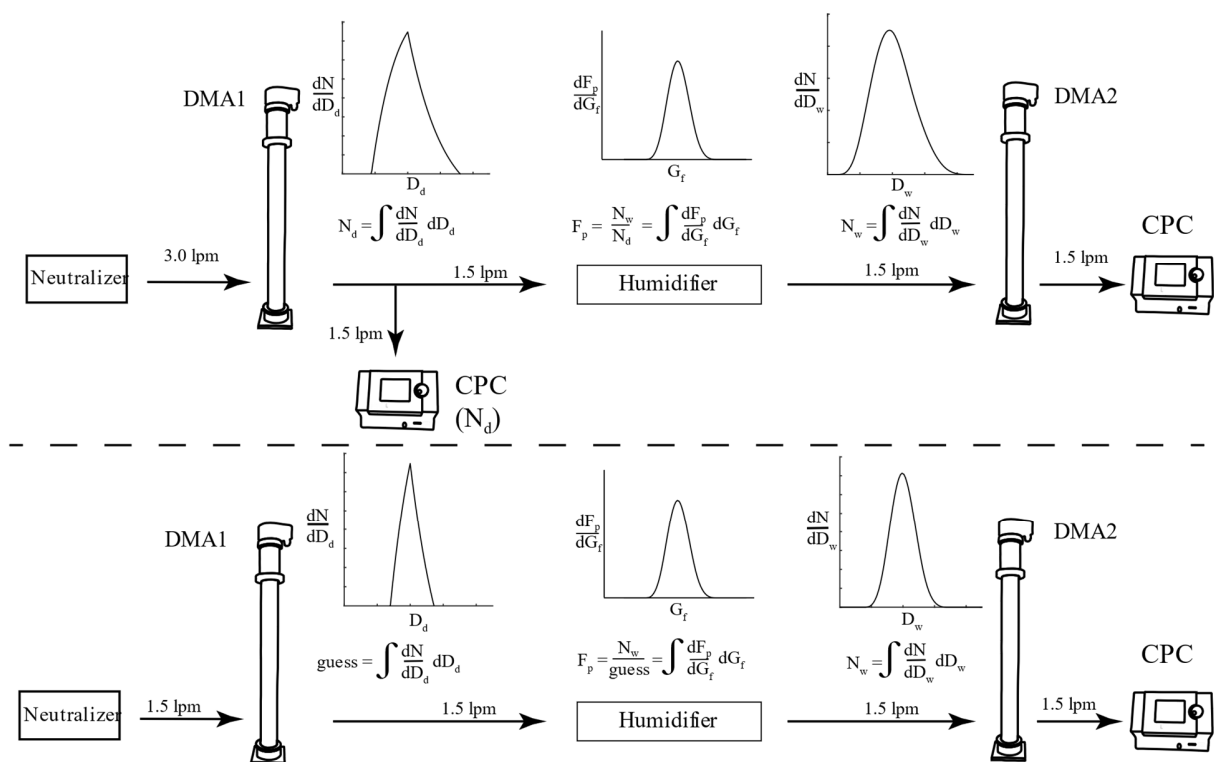


Figure 1. Comparison between an H-TDMA with and without a DMA1 CPC. Removal of the DMA1 CPC narrows the DMA1 transfer function and makes the penetration fraction unmeasurable. Definitions of the variables can be found in Section 2.

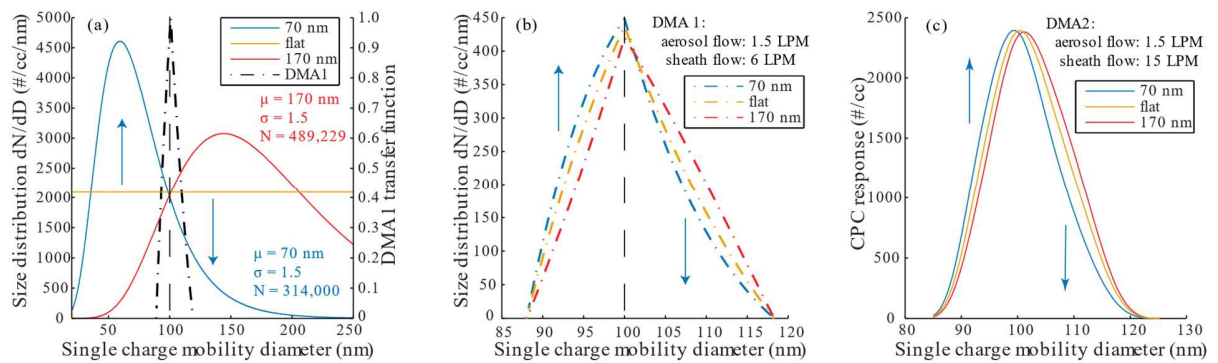


Figure 2. The influence of the inlet size distribution on the selected size distributions. The population of the blue inlet size distribution is higher than the flat size distribution (orange) on the left side of the transfer function and lower on the right side of the transfer function. This difference in population alters the shape of the selected size distribution as shown in panel (b). DMA2's interpretation of the response also shifts vertically, but this vertical shift appears to be horizontal in mobility diameter as shown in (c). The DMA1 transfer function in this example results from an aerosol:sheath flow ratio of 1:4, and a voltage set to select 100 nm singly-charged particles. The mean of the log-normal size distribution is μ , the standard deviation of the log-normal size distribution is σ , and N is the total number of particles in the inlet size distribution.

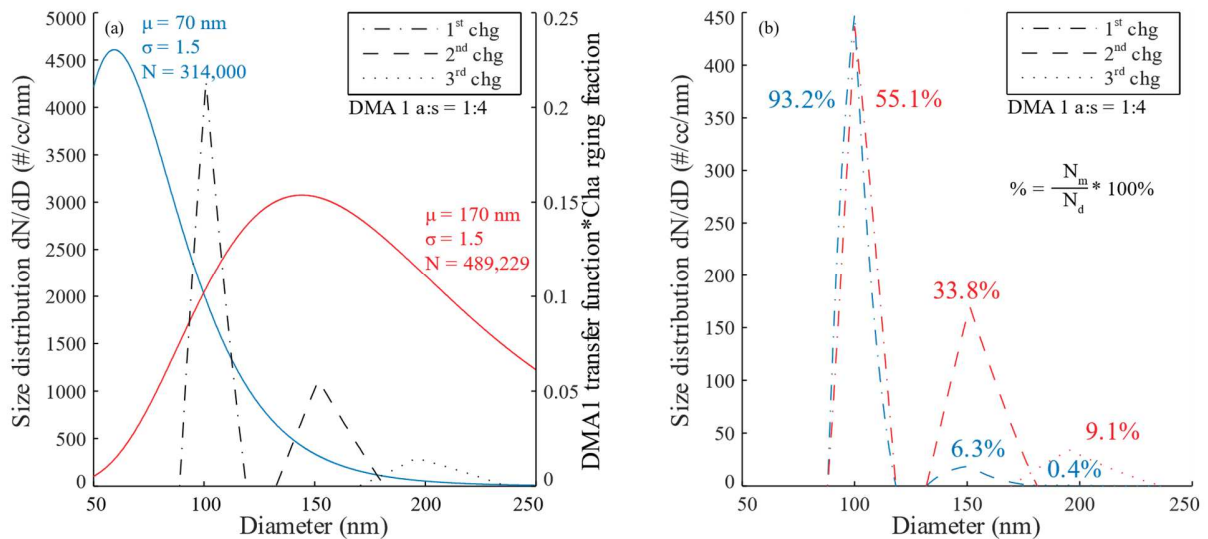


Figure 3. The first three transfer functions in DMA1 are plotted in panel (a). These transfer functions are plotted as the product of the transfer function and the charging fraction. Each selected size distribution is under the influence of its own Slope bias. For the blue inlet size distribution, all selected size distributions have negative Slope bias. For the red size distribution, the singly-charged selected size distribution has positive bias, the doubly-charged selected size distribution has neutral bias, and the triply-charged selected size distribution has negative bias. Just as was the case in Figure 2, here the DMA1 transfer

function results from an aerosol:sheath flow ratio of 1:4, and a voltage set to select 100 nm singly-charged particles. N_c is the total number of particles within a charge's selected size distribution. N_T is the total number of particles in all selected size distributions.

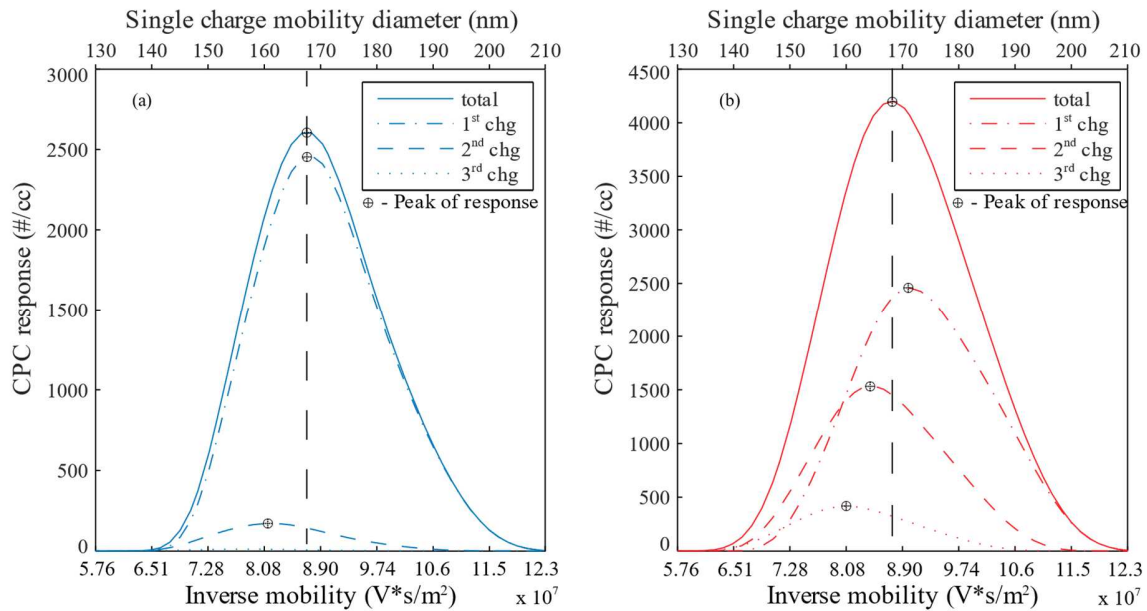


Figure 4. Modeled growth of selected size distributions from Figure 3(b) assuming the aerosol is ammonium sulfate at 90% relative humidity. Panel (a) is generated from the blue size distribution from Figure 3, and panel (b) is generated from the red size distribution from Figure 3. The shape of the two total CPC responses is similar, however, the reason for the shapes is very different.

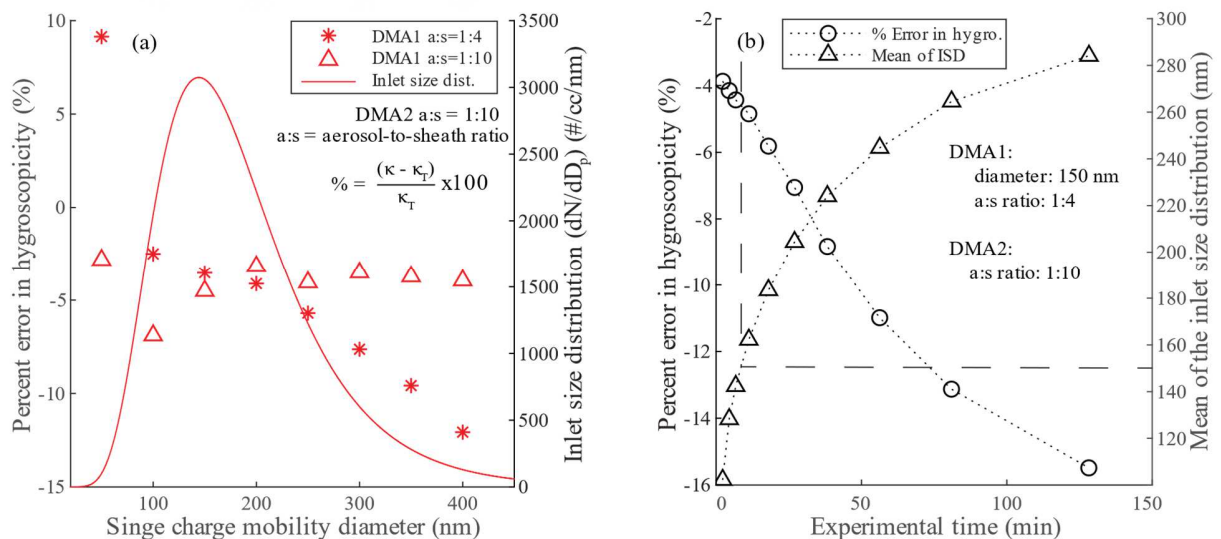


Figure 5. The modeled experimental response for two different experiments assuming growth of ammonium sulfate after increasing the relative humidity to 90%. In panel a, the hygroscopicity, κ , is

calculated for various DMA1 set points and compared to ideal. In panel b, the DMA1 transfer function is held constant, and the inlet size distribution evolves in a chamber as a function of time, while again comparing the hygroscopicity to ideal. The horizontal dashed line in panel (b) represent the DMA1 set point, and the vertical dashed line is added for readability. Ideal is defined as the hygroscopicity, κ_T , calculated using the DMA1 centroid and Tang and Munkelwitz (1994) empirical relationship. The investigation in panel (a) shows hygroscopicity is a function of diameter (See further discussion in *Supplemental Information S8*), and panel (b) shows hygroscopicity is a function of time. Technically, the hygroscopicity is constant throughout the model.

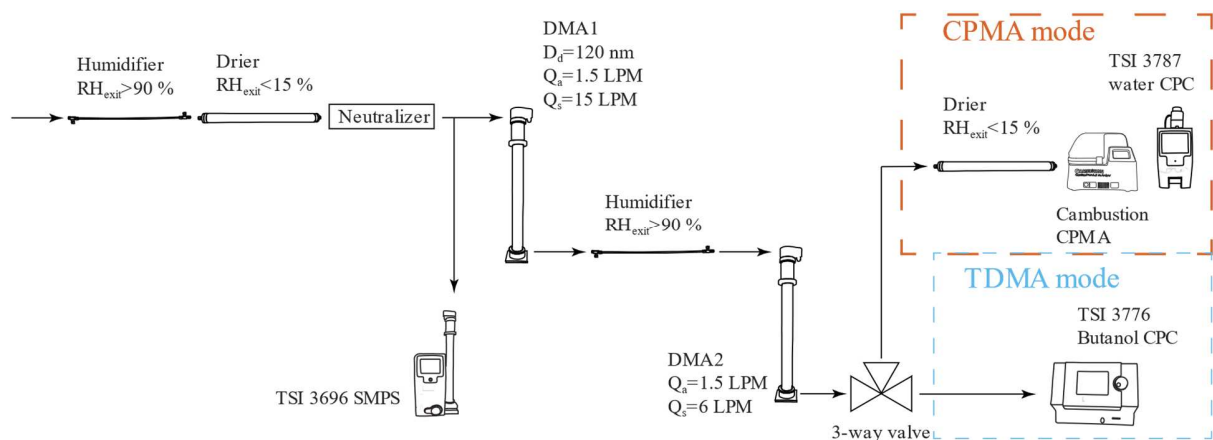


Figure 6. TDMA apparatus used to attribute the TDMA mode CPC response to each of the first three charges. When the flow, exiting DMA2, is passed to the TSI 3776 CPC, DMA2 scans normally. When the flow, exiting DMA2, is passed to the CPMA, DMA2 voltage is constant.

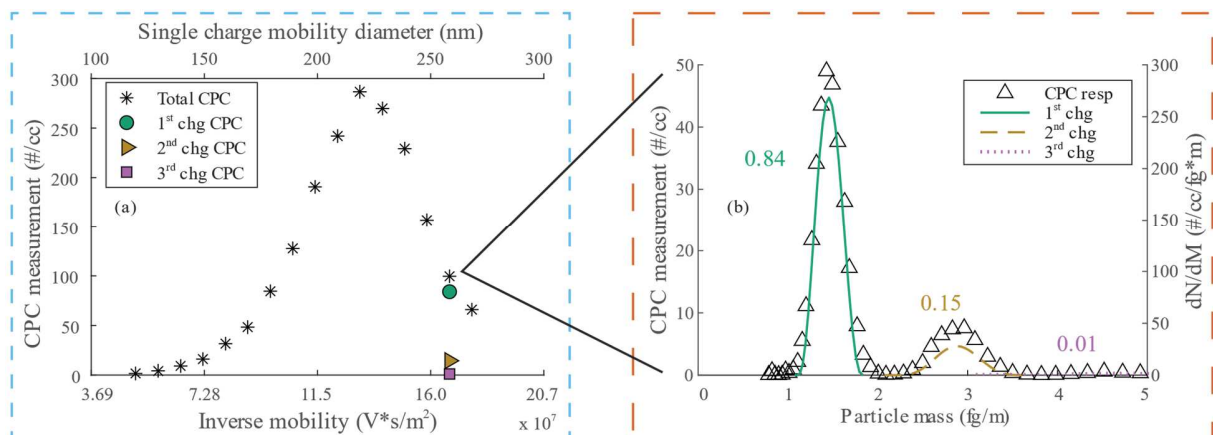


Figure 7. The two scanning modes used in the experiment. Panel (a) is a typical TDMA mode response for the humidified 120 nm grass burning aerosol. Panel (b) is a typical CPMA mode response from a selected DMA2 setting. The lines in panel b are the CPMA inversion of the CPC measurement. The fractions shown in panel (b) are the number of particles in each charge's mass distribution divided by the total number of particles. These fractions are multiplied by each of the TDMA mode CPC responses.

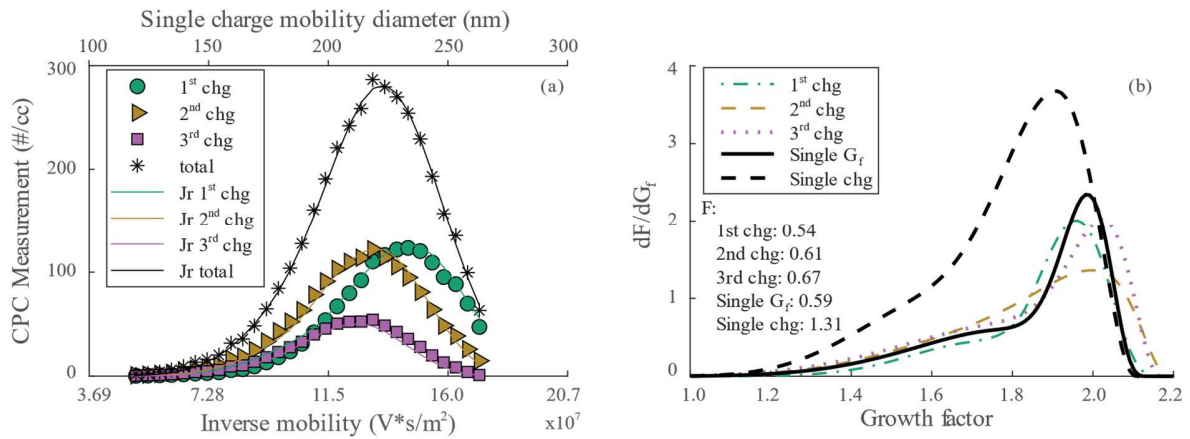


Figure 8 Experimental responses. Panel (a) is the DMA2 CPC response allotted to singly-, doubly-, and triply-charged particles. Panel (a) displays the three charges misalign, and therefore, grow to different sizes in DMA2 mobility space. Panel (b) is the inverted growth factor distributions from the CPC responses in panel (a). Listed below the legend are the penetration fractions (F) displayed per charge and overall assuming either a single growth factor distribution is representative of the population or a single charge is representative of the population.

11. Tables

Table 1. The value of the regularization multiplier for different values of $R_{CPC,n}$.

$R_{CPC,n}$ condition	γ value
$R_{CPC,n} < 0.05$	8
$0.05 < R_{CPC,n} < 0.25$	5
$0.25 < R_{CPC,n} < 0.5$	2
$R_{CPC,n} > 0.5$	1

Table 2. The first three charge diameters corresponding with the DMA1 centroid in Figure 3. Particles of these sizes experience the same growth factor (1.7) but do not grow equally in single charge diameter space.

	Dry size (nm)	Wet size (nm)	Equivalent +1 charge size (nm) (after growth)	Equivalent +1 charge (apparent) growth factor
Singly charged	100	170	170	1.7
Doubly charged	151.1	256.9	162.7	1.63
Triply charged	195.4	332.2	158.1	1.58

12. References

- Alroe, J., Cravigan, L. T., Mallet, M. D., Ristovski, Z. D., Miljevic, B., Osuagwu, C. G., & Johnson, G. R. (2018). Determining the link between hygroscopicity and composition for semi-volatile aerosol species. *Atmospheric Measurement Techniques*, *11*(7), 4361-4372.
- Baron, P. A. (2005). *Aerosol measurement principles, techniques, and applications* (2nd rev. ed.). Hoboken, NJ: Wiley.
- Carrico, C., Petters, M., Kreidenweis, S., Sullivan, A., McMeeking, G., Levin, E., . . . Collett Jr, J. (2010). Water uptake and chemical composition of fresh aerosols generated in open burning of biomass. *Atmospheric Chemistry and Physics*, *10*(11), 5165-5178.
- Chuang, P. Y., Nenes, A., Smith, J. N., Flagan, R. C., & Seinfeld, J. H. (2000). Design of a CCN instrument for airborne measurement. [Article]. *Journal of Atmospheric and Oceanic Technology*, *17*(8), 1005-1019. doi: 10.1175/1520-0426(2000)017<1005:Doacif>2.0.Co;2
- Cubison, M., Coe, H., & Gysel, M. (2005). A modified hygroscopic tandem DMA and a data retrieval method based on optimal estimation. *Journal of aerosol science*, *36*(7), 846-865.
- Farmer, D. K., Cappa, C. D., & Kreidenweis, S. M. (2015). Atmospheric processes and their controlling influence on cloud condensation nuclei activity. *Chemical Reviews*, *115*(10), 4199-4217.
- Friedlander, S. K. (2000). *Smoke, dust, and haze : fundamentals of aerosol dynamics* (2nd ed.). New York: Oxford University Press.
- Gunn, R. (1956). The Hyperelectrification of Raindrops by Atmospheric Electric Fields. *Journal of Meteorology*, *13*(3), 283-288. doi: Doi 10.1175/1520-0469(1956)013<0283:Thorba>2.0.Co;2
- Gysel, M., McFiggans, G., & Coe, H. (2009). Inversion of tandem differential mobility analyser (TDMA) measurements. *Journal of Aerosol Science*, *40*(2), 134-151.
- Hakala, J., Mikkilä, J., Hong, J., Ehn, M., & Petäjä, T. (2017). VH-TDMA: A description and verification of an instrument to measure aerosol particle hygroscopicity and volatility. *Aerosol Science and Technology*, *51*(1), 97-107.
- Hennig, T., Massling, A., Brechtel, F., & Wiedensohler, A. (2005). A tandem DMA for highly temperature-stabilized hygroscopic particle growth measurements between 90% and 98% relative humidity. *Journal of Aerosol Science*, *36*(10), 1210-1223.
- Johnson, G. R., Fletcher, C., Meyer, N., Modini, R., & Ristovski, Z. D. (2008). A robust, portable H-TDMA for field use. [Article]. *Journal of Aerosol Science*, *39*(10), 850-861. doi: 10.1016/j.jaerosci.2008.05.005
- Kelly, J. T., Wexler, A. S., Chan, C. K., & Chan, M. N. (2008). Aerosol thermodynamics of potassium salts, double salts, and water content near the eutectic. *Atmospheric environment*, *42*(16), 3717-3728.
- Kim, J. H., Mulholland, G. W., Kukuck, S. R., & Pui, D. Y. (2005). Slip correction measurements of certified PSL nanoparticles using a nanometer differential mobility analyzer (nano-DMA) for Knudsen number from 0.5 to 83. *Journal of Research of the National Institute of Standards and technology*, *110*(1), 31.
- Knutson, E., & Whitby, K. (1975). Aerosol classification by electric mobility: apparatus, theory, and applications. *Journal of Aerosol Science*, *6*(6), 443-451.
- Köhler, H. (1936). The nucleus in and the growth of hygroscopic droplets. *Transactions of the Faraday Society*, *32*, 1152-1161.
- Levin, E., McMeeking, G., Carrico, C., Mack, L., Kreidenweis, S., Wold, C., . . . Collett Jr, J. (2010). Biomass burning smoke aerosol properties measured during Fire Laboratory at Missoula Experiments (FLAME). *Journal of Geophysical Research: Atmospheres*, *115*(D18).
- Lewis, K., Arnott, W., Moosmüller, H., Chakrabarty, R., Carrico, C., Kreidenweis, S., . . . Jimenez, J. (2009). Reduction in biomass burning aerosol light absorption upon humidification: roles of

- inorganically-induced hygroscopicity, particle collapse, and photoacoustic heat and mass transfer. *Atmospheric Chemistry and Physics*, 9(22), 8949-8966.
- Liu, B., Pui, D., Whitby, K., Kittelson, D. B., Kousaka, Y., & McKenzie, R. (1978). The aerosol mobility chromatograph: a new detector for sulfuric acid aerosols *Sulfur in the Atmosphere* (pp. 99-104): Elsevier.
- Lopez-Yglesias, X. F., Yeung, M. C., Dey, S. E., Brechtel, F. J., & Chan, C. K. (2014). Performance Evaluation of the Brechtel Mfg. Humidified Tandem Differential Mobility Analyzer (BMI HTDMA) for Studying Hygroscopic Properties of Aerosol Particles. [Article]. *Aerosol Science and Technology*, 48(9), 969-980. doi: 10.1080/02786826.2014.952366
- Martin, M., Tritscher, T., Juranyi, Z., Heringa, M. F., Sierau, B., Weingartner, E., . . . Baltensperger, U. (2013). Hygroscopic properties of fresh and aged wood burning particles. *Journal of Aerosol Science*, 56, 15-29.
- McMurry, P. H., & Stolzenburg, M. R. (1989). On the Sensitivity of Particle-Size to Relative-Humidity for Los-Angeles Aerosols. *Atmospheric Environment*, 23(2), 497-507. doi: Doi 10.1016/0004-6981(89)90593-3
- Nah, T., McVay, R. C., Pierce, J. R., Seinfeld, J. H., & Ng, N. L. (2017). Constraining uncertainties in particle-wall deposition correction during SOA formation in chamber experiments. *Atmospheric Chemistry and Physics*, 17(3), 2297-2310.
- Olfert, J., & Collings, N. (2005). New method for particle mass classification—the Couette centrifugal particle mass analyzer. *Journal of Aerosol Science*, 36(11), 1338-1352.
- Oxford, C. R., Rapp, C. M., Wang, Y., Kumar, P., Watson, D., Portelli, J. L., . . . Williams, B. J. (2019). Development and qualification of a VH-TDMA for the study of pure aerosols. *Aerosol Science and Technology*, 53(2), 120-132.
- Petters, M. D. (2018). A language to simplify computation of differential mobility analyzer response functions. *Aerosol Science and Technology*, 52(12), 1437-1451.
- Petters, M. D., & Kreidenweis, S. (2007). A single parameter representation of hygroscopic growth and cloud condensation nucleus activity. *Atmospheric Chemistry and Physics*, 7(8), 1961-1971.
- Rader, D., & McMurry, P. (1986). Application of the tandem differential mobility analyzer to studies of droplet growth or evaporation. *Journal of Aerosol Science*, 17(5), 771-787.
- Regayre, L., Pringle, K., Booth, B., Lee, L., Mann, G., Browse, J., . . . Carslaw, K. (2014). Uncertainty in the magnitude of aerosol-cloud radiative forcing over recent decades. *Geophysical Research Letters*, 41(24), 9040-9049.
- Roberts, G. C., & Nenes, A. (2005). A continuous-flow streamwise thermal-gradient CCN chamber for atmospheric measurements. [Article]. *Aerosol Science and Technology*, 39(3), 206-221. doi: 10.1080/027868290913988
- Schwartz, S. E. (2018). Unrealized global temperature increase: Implications of current uncertainties. *Journal of Geophysical Research: Atmospheres*, 123(7), 3462-3482.
- Schwartz, S. E., Charlson, R. J., Kahn, R. A., Ogren, J. A., & Rodhe, H. (2010). Why hasn't Earth warmed as much as expected? *Journal of Climate*, 23(10), 2453-2464.
- Snider, J. R., Petters, M. D., Wechsler, P., & Liu, P. S. K. (2006). Supersaturation in the Wyoming CCN instrument. [Article]. *Journal of Atmospheric and Oceanic Technology*, 23(10), 1323-1339. doi: 10.1175/jtech1916.1
- Stocker, T. F., Qin, D., Plattner, G.-K., Tignor, M. M., Allen, S. K., Boschung, J., . . . Midgley, P. M. (2014). Climate Change 2013: The physical science basis. contribution of working group I to the fifth assessment report of IPCC the intergovernmental panel on climate change: Cambridge University Press.
- Stolzenburg, M. R. (2018). A review of transfer theory and characterization of measured performance for differential mobility analyzers. *Aerosol Science and Technology*, 52(10), 1194-1218.
- Stolzenburg, M. R., & McMurry, P. H. (2008). Equations governing single and tandem DMA configurations and a new lognormal approximation to the transfer function. *Aerosol Science and Technology*, 42(6), 421-432.

- Stratmann, F., Orsini, D., & Kauffeldt, T. (1997). Inversion algorithm for TDMA measurements. *Journal of Aerosol Science*, *1001*(28), S701-S702.
- Swietlicki, E., Hansson, H.-C., Hämeri, K., Svenningsson, B., Massling, A., McFiggans, G., . . . Gysel, M. (2008). Hygroscopic properties of submicrometer atmospheric aerosol particles measured with H-TDMA instruments in various environments—a review. *Tellus B: Chemical and Physical Meteorology*, *60*(3), 432-469.
- Tang, I., & Munkelwitz, H. (1994). Water activities, densities, and refractive indices of aqueous sulfates and sodium nitrate droplets of atmospheric importance. *Journal of Geophysical Research: Atmospheres*, *99*(D9), 18801-18808.
- Tritscher, T., Dommen, J., DeCarlo, P., Gysel, M., Barmet, P., Praplan, A., . . . Donahue, N. (2011). Volatility and hygroscopicity of aging secondary organic aerosol in a smog chamber. *Atmospheric Chemistry and Physics*, *11*(22), 11477-11496.
- Varutbangkul, V., Brechtel, F., Bahreini, R., Ng, N., Keywood, M., Kroll, J., . . . Goldstein, A. (2006). Hygroscopicity of secondary organic aerosols formed by oxidation of cycloalkenes, monoterpenes, sesquiterpenes, and related compounds. *Atmospheric Chemistry and Physics*, *6*(9), 2367-2388.
- Villani, P., Picard, D., Michaud, V., Laj, P., & Wiedensohler, A. (2008). Design and validation of a volatility hygroscopic tandem differential mobility analyzer (VH-TDMA) to characterize the relationships between the thermal and hygroscopic properties of atmospheric aerosol particles. [Article]. *Aerosol Science and Technology*, *42*(9), 729-741. doi: 10.1080/02786820802255668
- Voutilainen, A., Stratmann, F., & Kaipio, J. (2000). A non-homogeneous regularization method for the estimation of narrow aerosol size distributions. *Journal of aerosol science*, *31*(12), 1433-1445.
- Wiedensohler, A. (1988). An approximation of the bipolar charge distribution for particles in the submicron size range. *Journal of Aerosol Science*, *19*(3), 387-389.